Theoretical and Applied Climatology (2025) 156:308
https://doi.org/10.1007/s00704-025-05509-9

RESEARCH

Effects of modifying surface sensible heat flux on summertime local precipitation in urban areas of Osaka, Japan

Kenta Irie[1] · Tetsuya Takemi[1]

Received: 25 February 2025 / Accepted: 22 April 2025

Abstract

Cumulonimbus clouds that develop rapidly during summertime afternoons can cause local heavy precipitation and local flooding, particularly in urban areas. This study examines the potential to mitigate the severity of urban precipitation by reducing sensible heat flux (SHF). Large SHF characterizes urban areas due to anthropogenic factors such as heat emissions from buildings and roads, leading to the urban heat island effect. To assess the impact of SHF reduction, numerical simulations for an afternoon precipitation event in Osaka, Japan were conducted using the Weather Research and Forecasting (WRF) model. The nesting capability was used to increase the horizontal resolution to 0.5 km in the innermost domain. SHF reduction experiments were conducted by varying the reduction levels of SHF against no-reduction experiment (CTL) (ranging from 50 to 90% of CTL) and the size of the region of SHF reduction (the entire innermost domain, only urban grids of the innermost domain, and urban grids within a 20 km box of innermost domain). We created CTL and 15 types of reduction experiments with 8 ensemble members initialized at different times for each and a total of 128 members were created. The control experiment (CTL) reproduced the actual afternoon precipitation event. Results showed that SHF reduction experiments suppressed accumulated and peak precipitation in most cases compared to CTL. Extreme precipitation events, defined as precipitation above the 99.9th percentile value in CTL, were also less frequent in most cases. The most practical reduction experiment, 10% reduction level in the 20-km box area, resulted in a decrease of 18% in accumulated precipitation, 13% in peak precipitation, and 9% in the 99.9th percentile value of precipitation. These findings indicate that the reduction of SHF would stabilize the lower troposphere and hence would lead to reducing cloud formation and precipitation. This study demonstrates a potential for reducing SHF as a measure to mitigate urban precipitation under accelerating urbanization.

1 Introduction

Cumulonimbus clouds, which develop rapidly in the afternoon during the summer season, can cause heavy precipitation and local flooding in a short time period. During sunny days when synoptic-scale disturbances such as tropical cyclones and fronts are not present, solar radiation heats the ground, generating favorable conditions for the initiation of convection. It is known that the atmospheric stability diagnosed by the vertical temperature gradient between the middle- and the lower-troposphere as well as the water vapor content plays a key role in causing afternoon precipitation (Nomura and Takemi 2011; Takemi 2014).

Yamamoto and Ishikawa (2020) investigated surface temperatures in the urban area of Osaka, Japan using the geostationary meteorological satellite Himawari-8. They found that daytime surface temperatures were higher in areas with a high density of low-rise buildings compared to areas with high-rise buildings or a low density of low-rise buildings, highlighting the impact of building density on diurnal surface temperature variations. Urban areas are characterized by larger sensible heat fluxes (SHF) than rural areas, owing to heat release from buildings, roads, and anthropogenically generated heat. Such enhanced heat fluxes are hypothesized to cause the urban heat islands (UHI) phenomena (Kanda 2007; Oke et al. 2017).

In urban areas, the boundary layer is warmed by the UHI, and the tropospheric stratification becomes unstable,

✉ Kenta Irie
irie_k@storm.dpri.kyoto-u.ac.jp

Tetsuya Takemi
takemi@storm.dpri.kyoto-u.ac.jp

[1] Disaster Prevention Research Institute, Kyoto University, Gokasho, Uji, Kyoto, Japan

Published online: 12 May 2025

suggesting that urban heating has some relationship with precipitation. The relationship between urban areas and precipitation has been studied for a long time in order to understand the effects of urbanization on precipitation. There have been some major field measurements conducted in St. Louis (METROMEX project, Changon et al. 1971) and in Atlanta (ATLANTA project, Quattrochi et al. 1998). Urban effects on precipitation are considered to be primarily due to the UHI (Oke et al. 2017), leading the precipitation downwind of urban areas (Bornstein and Lin 2000; Shem and Shepherd 2009; Han and Baik 2008).

Recent studies have investigated the changes of extreme precipitation in urban areas in the future climate (Doan et al. 2022; Steensen et al. 2022). Doan et al. (2022) suggested that precipitation under global warming conditions increased by temporarily suppressing convection before it occurs. Specifically, global warming enhances convective inhibition, which delays the initiation of convection by preventing weaker convective updrafts from forming. During this suppression period, surface heating continues, leading to an accumulation of convective available potential energy. Once the inhibition is overcome, the stored energy is released more abruptly, generating stronger convective updrafts and more intense precipitation. Therefore, controlling the amount of precipitation, especially extreme precipitation, can be made possible by exploring ways to mitigate surface heat in urban areas.

Fujibe et al. (2009) noted an increasing trend in precipitation during the warm season in Tokyo and pointed out that it was caused by the effects of the UHI. Most previous studies on UHI-induced precipitation have focused on Tokyo (Fujibe 1998; Kusaka et al. 2000, 2014; Seino et al. 2018), while ignoring other metropolitan areas such as Osaka, which is the third largest commercial city in Japan and is characterized by a large population density and high density of buildings (Statistics Bureau of Japan 2025). Takemi et al. (2020) studied building parameters in Kyoto, Osaka, and Tokyo, and found that Osaka has comparable characteristics to Tokyo, suggesting the importance of research in Osaka. In previous studies on urbanization and precipitation, numerical simulations were performed for cases that occur in different land use categories, such as urban, forest, and paddy fields (Matheson and Ahsie 2008; Shimadera et al. 2015). The results of these simulations showed that urbanization increases SHF and precipitation. Those simulation studies showed that precipitation decreased when urban land use categories were changed to non-urban land use, indicating an increase in precipitation due to urbanization. Shimadera et al. (2015) performed numerical simulations for precipitation events in Osaka with varying land use categories and concluded that an increase in precipitation due to urbanization was attributed to SHF that promoted the formation and development of convective clouds.

In this way, most studies have focused on the impacts of urbanization on precipitation by examining the influence of land use. However, few studies have focused on the changes of precipitation in urban areas through artificial modifications and/or interventions such as reducing heat release from urban surfaces (e.g., painting building roofs white and/or rooftop greening). The Japanese Cabinet Office has initiated a challenging research project of weather control and modification under the Moonshot Research and Development Program Goal 8 since 2023. The goal of this project is to control increasingly intense heavy rainfall and realize a safe and secure society without the threat of strong winds and flooding by 2050. One of the goals of this program is to control the rapid development of thunderstorms in urban areas in summertime afternoon periods. Previous studies have found a positive relationship between SHF and precipitation, however, these studies only looked at the impact of SHF on precipitation with changing the land use categories in terms of urbanization. On the other hand, it is uncertain how much this relationship will change if we only modify the SHF emitted by urban areas while keeping other land use categories constant. Also, the quantitative relationship between SHF changes and precipitation changes has not been indicated.

This study focuses on the impact of modifying the region and reduction level of SHF amount on precipitation in urban areas and aims to demonstrate quantitively the potential for suppression of urban precipitation through SHF modification. Section 2 describes the selected case, the model configuration, and the setup of the experiments with SHF modification. Section 3 describes the results of the experiment without SHF modification, and the results of the reduction experiment are provided in Sect. 4. The mechanism of precipitation suppression is discussed in Sect. 5, and the conclusions of this study are presented in Sect. 6.

2 Method

2.1 Selection of a case

The phenomenon targeted in this study is a local-scale precipitation event caused by rapidly developing cumulonimbus clouds during the daytime in summer over urban areas in Osaka. First, here we describe the method used to select a case. We focus on recent local-scale precipitation events in Osaka, and thus we look for cases in July, August, and September in years from 2020 to 2023. The radar data with 1 km resolution provided by the Japan Meteorological Agency (JMA) are used to detect thunderstorms and also to validate the results of numerical simulations. Figure 1 shows, as an example, the time series of the horizontal distribution of precipitation calculated from the radar reflectivity from 1330 Japan Standard Time (hereafter referred to as JST, which is UTC + 9 h) to 1430 JST 27 August 2023. This figure also shows the method used to extract cumulonimbus clouds. A 1° × 1° box area centered on the Automated Meteorological Data Acquisition System (AMeDAS) point in Osaka (34.68°N, 135.52°E) was selected to cover precipitation in central area of Osaka. Circular regions with radius of 10 km and 20 km centered at the Osaka AMeDAS point were applied; each region was referred to as R10 and R20, respectively.

The conditions for extracting cumulonimbus clouds using these regions were as follows:

1) There is a signal greater than 10 mm h^{-1} within R10 at the arbitrary time T.
2) There is no signal exceeding 1 mm h^{-1} within R20 at 30 min before the time T.
3) There is a signal greater than 10 mm h^{-1} in R10 until 30 min after the time T.
4) The extraction time is between 1200 JST and 1700 JST,
5) There are no synoptic-scale disturbances such as fronts and tropical cyclones within 5 degrees of latitude and longitude from the AMeDAS point.

These five conditions ensure that we detect separate local precipitation events that rapidly develop within 30 min surrounding the Osaka urban area. With this procedure, we found fifteen cases. Among these fifteen extracted cases, we subjectively excluded fast-moving or organized cases by visual examinations and finally selected the case of 27 August 2023. We confirmed that this day had a typical summer environmental field where there were no significant synoptic-scale disturbances, using weather maps provided by JMA. Precipitation observed at the AMeDAS at 1330 JST was weak by 1350 JST, but stationary and strong precipitation developed to the east-southeast of the AMeDAS until 1410 JST, which finally became weaker. The numerical model used in this study was designed to simulate such precipitation with a small spatiotemporal scale.

2.2 Configuration of the numerical model

The model used in this study was the Weather Research and Forecasting (WRF) Model Version 4.1.3 (Skamarock et al. 2019). The simulation had three two-way-nested domains. Domain 1 covered the area of Japan and the surroundings (D01, Fig. 2a, black box), Domain 2 covered the Kyushu to Tohoku region (D02, Fig. 2a, blue box), and Domain 3 covered the Kinki region centered at the Osaka AMeDAS point (D03, Fig. 2a and b, red box). Time steps for temporal integration were set to 18, 6, and 2 s for D01, D02, and D03, respectively. The horizontal resolutions and the numbers of horizontal grid points were 4.5 km and 899 × 899, 1.5 km and 702 × 702, and 0.5 km and 411 × 411 for D01, D02, and D03, respectively. Since increasing the number of the vertical resolution allows a more detailed representation of convection and wet processes such as condensation

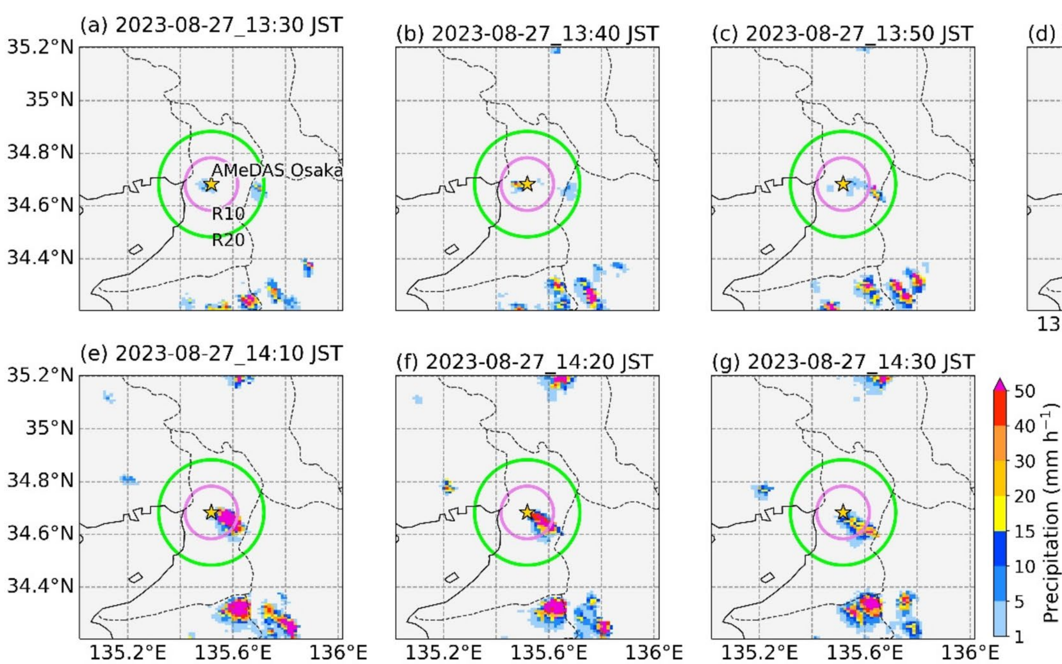

Fig. 1 Development of radar reflectivity (shaded) for the case used in this study from 1330 JST to 1430 JST 27 August 2023. The pink (green) circle is the R10 (R20) and the yellow star indicates the Osaka AMeDAS point

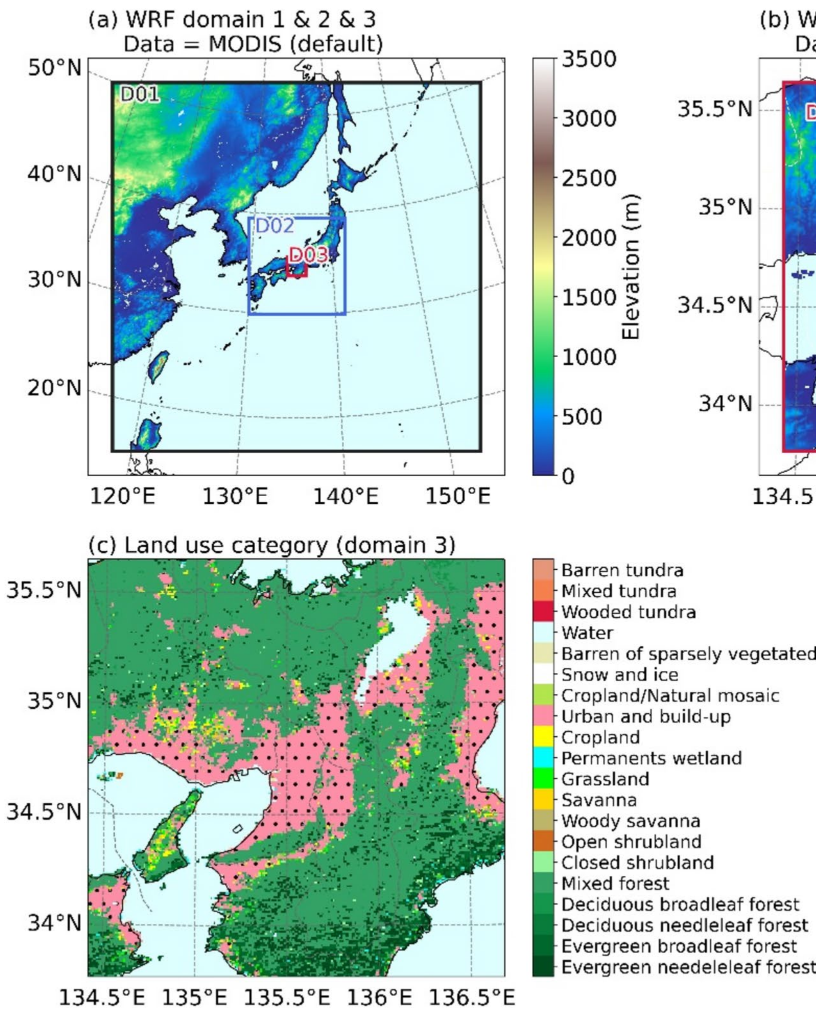

Fig. 2 (**a**) All the domains, (**b**) Domain 3 and the shaded shows the terrain height (m). The land use category is shown in (**c**). The yellow star in (**b**) indicates the Osaka AMeDAS point, and the dotted area in (**c**) is the urban land use category

and evaporation, there is the potential for improved distribution and accuracy of locally heavy precipitation (Aligo et al. 2009). Therefore we used hybrid vertical coordinates with denser settings for the lower layers. The vertical coordinates had 70 sigma pressure levels from the surface to the level of 20 hPa, which results in the lowest model-height of approximately 55 m averaged over R20 in D03. As the resolution of the topographic data is related to the reproducibility of local circulation and precipitation (Takemi 2009a, b, 2018; Takemi and Ito 2020), the dataset of Digital Map 50 m Grid (Elevation) produced by the Geospatial Information Authority of Japan (referred as GIA50) was used only for D03. For the initial and boundary values, we used the European Center for Medium-term Forecasts (ECMWF) fifth-generation global reanalysis (ERA5; Hersbach et al. 2020) which has 0.25°×0.25° horizontal resolution and 1-hour time interval. The time interval of simulated output data is 10 min in D03.

The physics schemes used in this study were Thompson 2-moment for the microphysics scheme, Mellor-Yamada-Nakanishi-Niino level-3 for the planetary boundary layer scheme, Rapid Radiative Transfer Model for Global Climate Models for the longwave/shortwave radiation scheme, and Unified Noah for the land surface model. The cumulus convection scheme and urban canopy model were not used in this study. In reproducing cumulonimbus clouds that develop in short time-scales, a single experiment has large uncertainties owing to a highly random nature of the occurrence of cumulonimbus clouds and their nonlinear response to the initial conditions and model configurations. Therefore, 8 ensemble members (control experiment; CTL) were created by varying the initial time of the time integration at 3-hour intervals from 0000 JST to 2100 JST 26 August 2023. With this ensemble members, their average (ensemble mean) was examined to estimate the uncertainty. The analysis period was from 0900 JST to 2100 JST 27 August 2023. In order to allow for shifts in locations of precipitation in each ensemble member, precipitation averaged over the R20 was used for the investigation.

Table 1 Combination of reduction area and reduction level

Reduction level	ALL	URB	O20
10%	ALL-09	URB-09	O20-09
20%	ALL-08	URB-08	O20-08
30%	ALL-07	URB-07	O20-07
40%	ALL-06	URB-06	O20-06
50%	ALL-05	URB-05	O20-05

2.3 Design of experiments reducing sensible heat flux

Experiments reducing SHF were conducted by applying a factor to the equation that calculates SHF in the Noah Land Surface Model. Reduction experiments were conducted as steady reduction of SHF throughout the entire period of the time integration. We assumed this reduction operation to be the decreasing SHF which would be achieved somehow through an artificial intervention (e.g., storing heat near the ground surface by thermal storage materials to reuse the heat by operating heat pumps). The same initial and boundary values as those in CTL were used for all the members of the reduction experiment. The members of reduction experiments were created by decreasing SHF from 10 to 50% by 10% relative to the SHF of CTL. In addition, members that reduced SHF for the entire D03 (referred as ALL), only the urban grid of the entire D03 (referred as URB), and only the urban grid within the 20 km box centered at the Osaka AMeDAS point (referred as O20) were created. These fifteen reduction experiments were compared to CTL for sensitivity analysis. Note that each reduction experiment consisted of 8 ensemble members initialized at the different times as well as CTL. Totally, we conducted 120 simulations for reduction cases. The naming rule of the present experiments was expressed combining the reduction region and level in this study (e.g., ALL-05 represents the experiment of ALL with a 50% reduction level, in other words, 90% SHF of CTL). The combinations of sensitivity simulations in this study are shown in Table 1.

To compare the results of urban surface conditions in CTL with the AMeDAS observation, 2-m temperature (°C), 2-m relative humidity, and 10-m wind speed are shown in Fig. 3. There are variations among members in 2-m temperature, 2-m relative humidity (%), and 10-m wind speed (m s^{-1}). However, the ensemble mean values of each variable in CTL were almost consistent with the observation values. Therefore, urban conditions were reproduced in this study without the urban canopy model. Also, we verified SHF and latent heat flux in CTL in reduction experiments. Figure 4 shows the timeseries of difference in ensemble mean values of SHF and latent heat flux in CTL and that in reduction experiments. Whereas SHF differences in ALL and URB were similar, SHF differences in O20 were less than difference in ALL and URB. In this study, we conducted experiments in which only the SHF was reduced in the Noah LSM. The energy balance changed with time integration, and latent heat flux also changed as a result of reducing SHF. However, while the change in SHF was on the order of 10–100 Wm^{-2}, the change in LH was only on the order of 1 Wm^{-2} (Fig. 4). Therefore, we considered that the change in precipitation in this study was mainly due to the effect of decreasing SHF and that the effect of the change in latent heat flux was limited.

Figure 5 shows the horizontal distribution of CTL, ALL-05, URB-05, and O20-05 averaged from 1300 JST to 1600

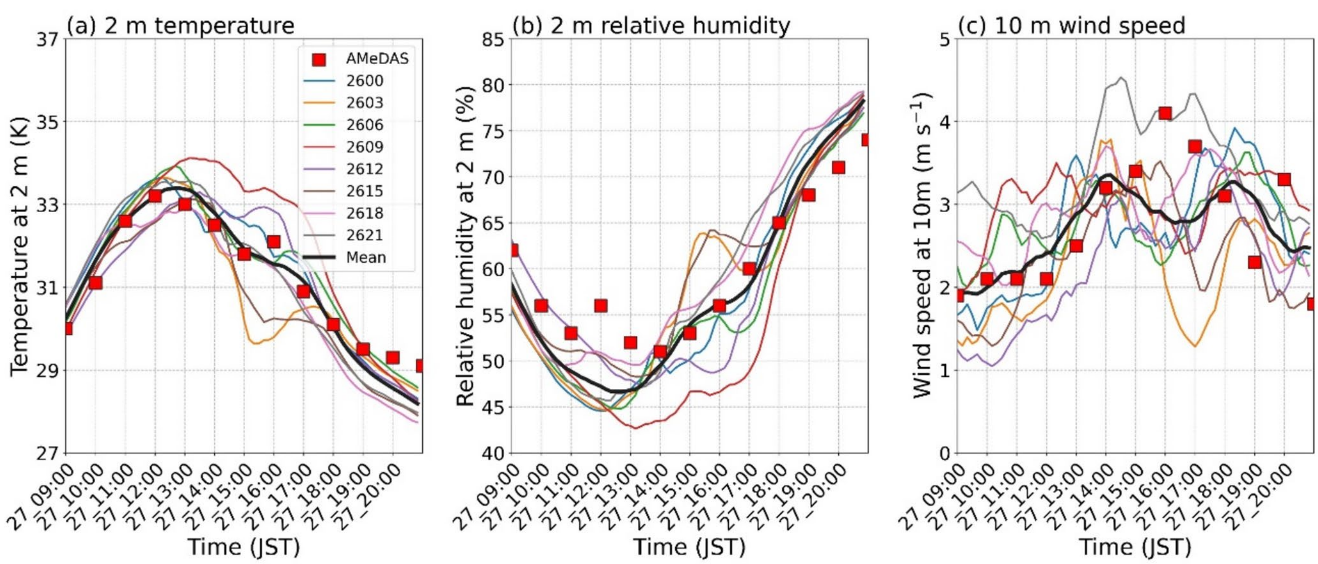

Fig. 3 Timeseries of (**a**) 2 m temperature (°C), (**b**) 2 m relative humidity (%), and (**c**) 10 m wind speed (m s^{-1}) in CTL. The red square marker indicates the observation value by AMeDAS, colors indicate the initial time period of integration for simulation, and the black solid line indicates the ensemble mean values

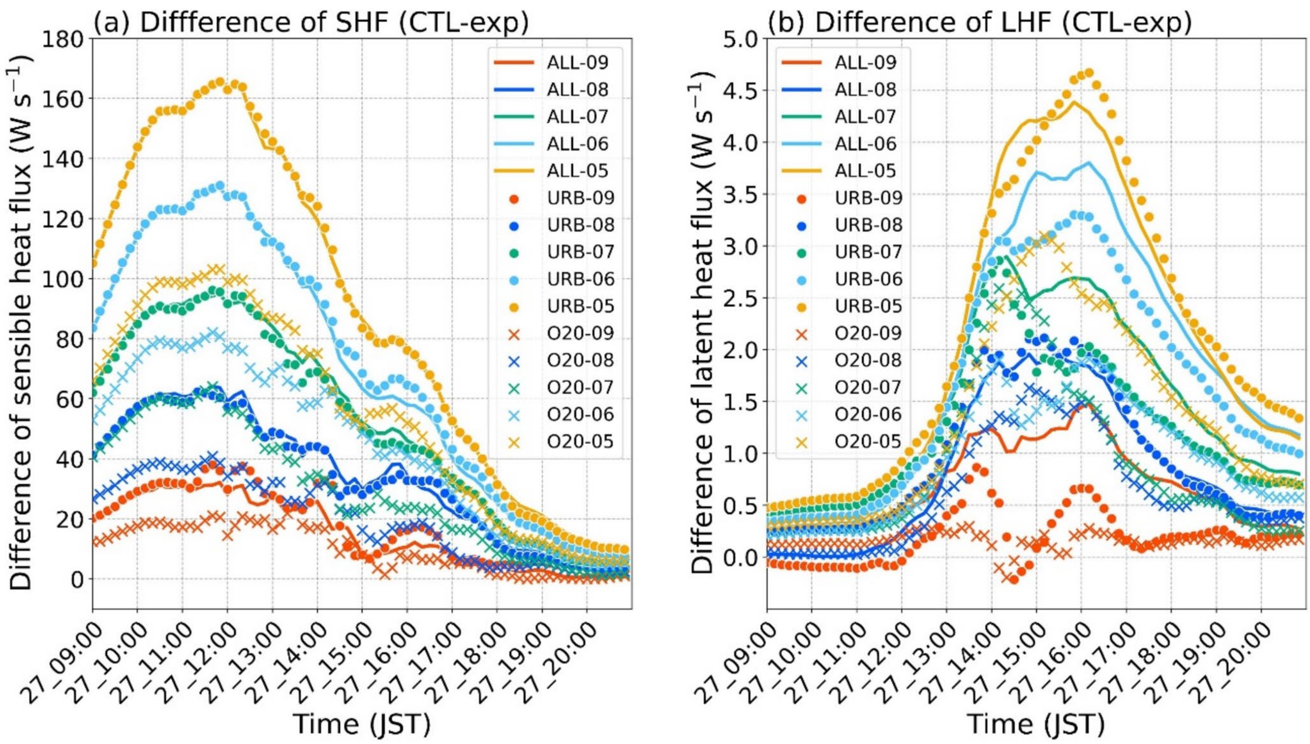

Fig. 4 Timeseries of the difference of (**a**) sensible heat flux and (**b**) latent heat flux between CTL and each reduction experiment. Each flux value is ensemble mean values. Colors indicate the reduction level. Solid lines, and dots, crosses indicate ALL, URB, and O20 experiment, respectively

JST 27 August 2023. Here we showed 50% experiments to demonstrate the differences between the cases. CTL showed that SHF was large in the urban grid (dotted hatch area) around AMeDAS, with a time-averaged value of over 200 W m^{-2} (Fig. 5a). SHF in urban grids was almost twice as large as that in the non-urban grids. Differences of the distribution of SHF were observed between coastal urban areas (e.g. Osaka Bay and Ise Bay) and from the southern part of Kyoto to the northern part of Nara (135.8°E, 34.7–35°N), and other areas. The areas with low SHF in the urban grid in Fig. 5a were considered to be due to the high frequency of precipitation and cooling of the land surface by precipitation.

3 Precipitation in CTL

This section describes the results of the precipitation reproduction of CTL. As mentioned in Sect. 2, CTL consists of 8 ensemble members created from 8 different initial times. Figure 6 shows the horizontal distribution of precipitation represented in terms of radar reflectivity for the members of CTL at 1410 JST 27 August 2023. Radar observation showed strong precipitation to the southeast of AMeDAS (Fig. 6a). Precipitation south of AMeDAS (around 135.5°E, 34°N) was enhanced by topography, and this precipitation appeared in all members (Fig. 6b-i). Cumulonimbus clouds within R20 appeared with sparse distribution in the numerical experiment. CTL was able to reproduce the atmospheric environmental field in which cumulonimbus clouds easily develop and thus to reproduce urban precipitation.

Figure 7a shows precipitation calculated from radar reflectivity and precipitation at the grid point closest to AMeDAS in CTL. As shown by the red squares in Fig. 7a, AMeDAS observed precipitation of 0.5 mm h^{-1} at 1400 JST and 1500 JST, while radar precipitation peaked at 1330 JST 27 August 2023. The difference in precipitation period between AMeDAS and radar observations was considered to be due to the fact that AMeDAS observes rainfall on the ground, while radar observes water droplets in the air, causing precipitation to evaporate before reaching the ground. The ensemble mean precipitation of CTL at the AMeDAS point had three peaks in the afternoon.

Figure 7b shows the precipitation averaged over urban grids within the R20. In the R20, precipitation by the radar observation peaked at 1410 JST 27 August 2023, while the ensemble mean precipitation of CTL peaked at 1440 JST on 27 August 2023. There was a little difference in peak times of precipitation; however, it was possible to use the R20 to examine afternoon precipitation in urban areas. The standard deviation for ensemble mean precipitation in the R20 at each time exceeded 0.1 mm h^{-1} at 1220 JST 27 August 2023 (marked by a star) and increased during the afternoon (Fig. 7c). This increase indicated that precipitation

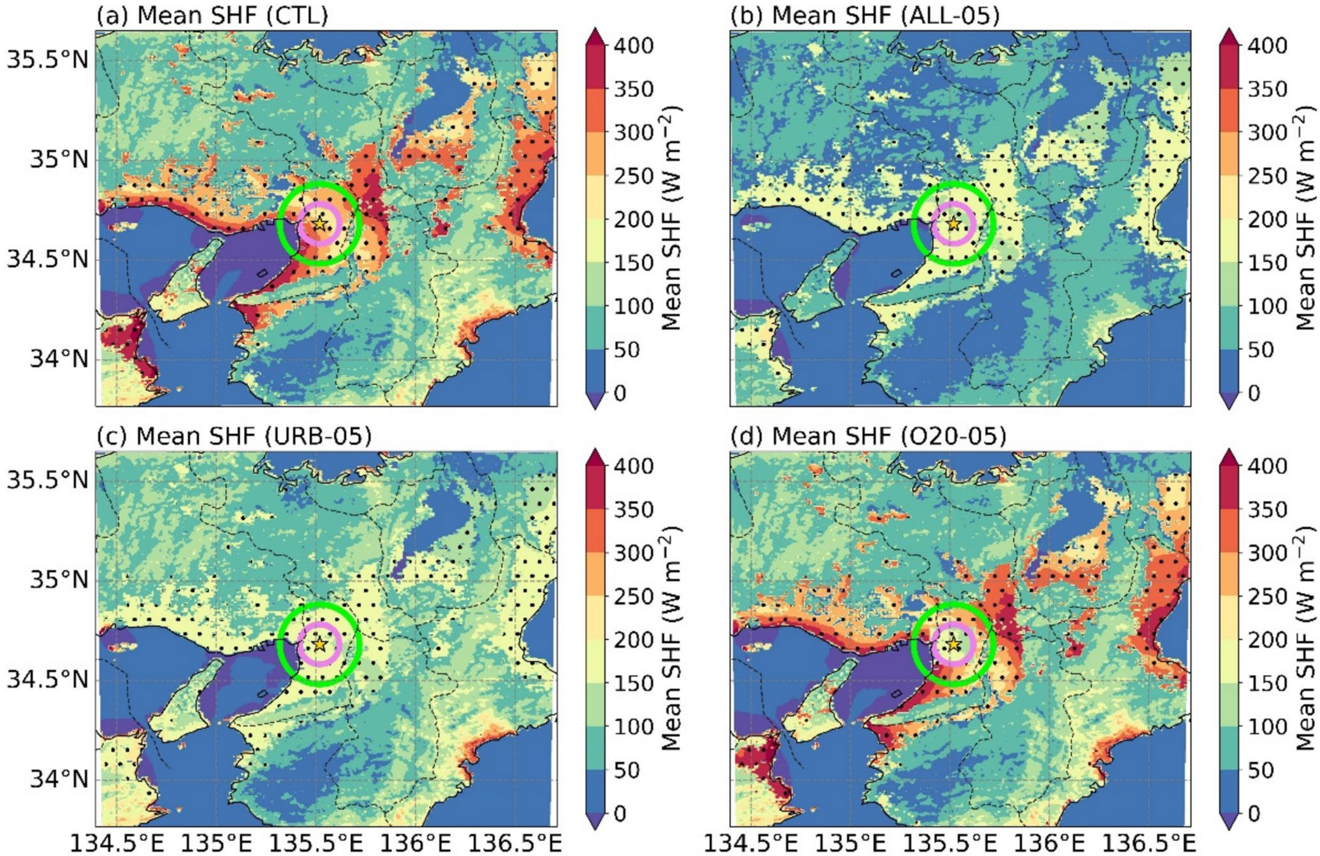

Fig. 5 Horizontal distribution of SHF modified with 50% in (**a**) CTL, (**b**) ALL, (**c**) URB, and (**d**) O20.The hatched area with dots indicates the urban category in the land use. The pink (green) circle is the R10 (R20) and the yellow star indicates the Osaka AMeDAS point. SHF value is averaged from 1300 JST to 1600 JST 27 August 2023

distribution and intensity differed among the ensemble members, indicating an uncertainty in the occurrence of precipitation increased in the afternoon. Accumulated ensemble mean precipitation started to increase from 1300 JST and remained constant after 1600 JST (Fig. 7d). The difference in accumulated precipitation for each member varied widely with a maximum value of 35 mm. Keeping in mind these characteristics of precipitation of CTL, the next section will examine the changes in precipitation due to the modification of SHF.

4 Comparison between CTL and reduction experiments

4.1 Accumulated and peak precipitation

We compared the characteristics of precipitation between the reduction experiments and CTL using ensemble mean accumulated and peak precipitation of the fifteen reduction experiments. Figure 8 shows the time series of ensemble mean precipitation averaged over the R20 for each sensitivity experiment. The solid line shows ensemble mean precipitation for each reduction experiment and the shading shows the standard deviation of precipitation among members. The values of accumulated precipitation are indicated in the left corner of each panel. ALL, URB, and O20 in all the reduction levels represented, to a certain degree, the afternoon peaks of precipitation as well as CTL. In ALL, both peak and accumulated precipitation were smaller than in CTL at all reduction levels (ALL-05 to ALL-09) (Fig. 8a). In URB, peak precipitation was larger than CTL in URB-09 and URB-07, while accumulated precipitation was smaller than CTL in all the modification ratios (URB-05 to URB-09) (Fig. 8b). In O20, as in ALL, both peak and accumulated precipitation were smaller than CTL (Fig. 8c). When all the experiments were compared at the same modification ratios, peak precipitations were similar for ALL, URB, and O20. In contrast, accumulated precipitations at the same modification ratios were comparable between ALL and URB, whereas it was larger in O20 compared to both ALL and URB. In each reduction experiment, the standard deviations of precipitation were largest in the afternoon among all the time period, and especially maximum in URB-07. In

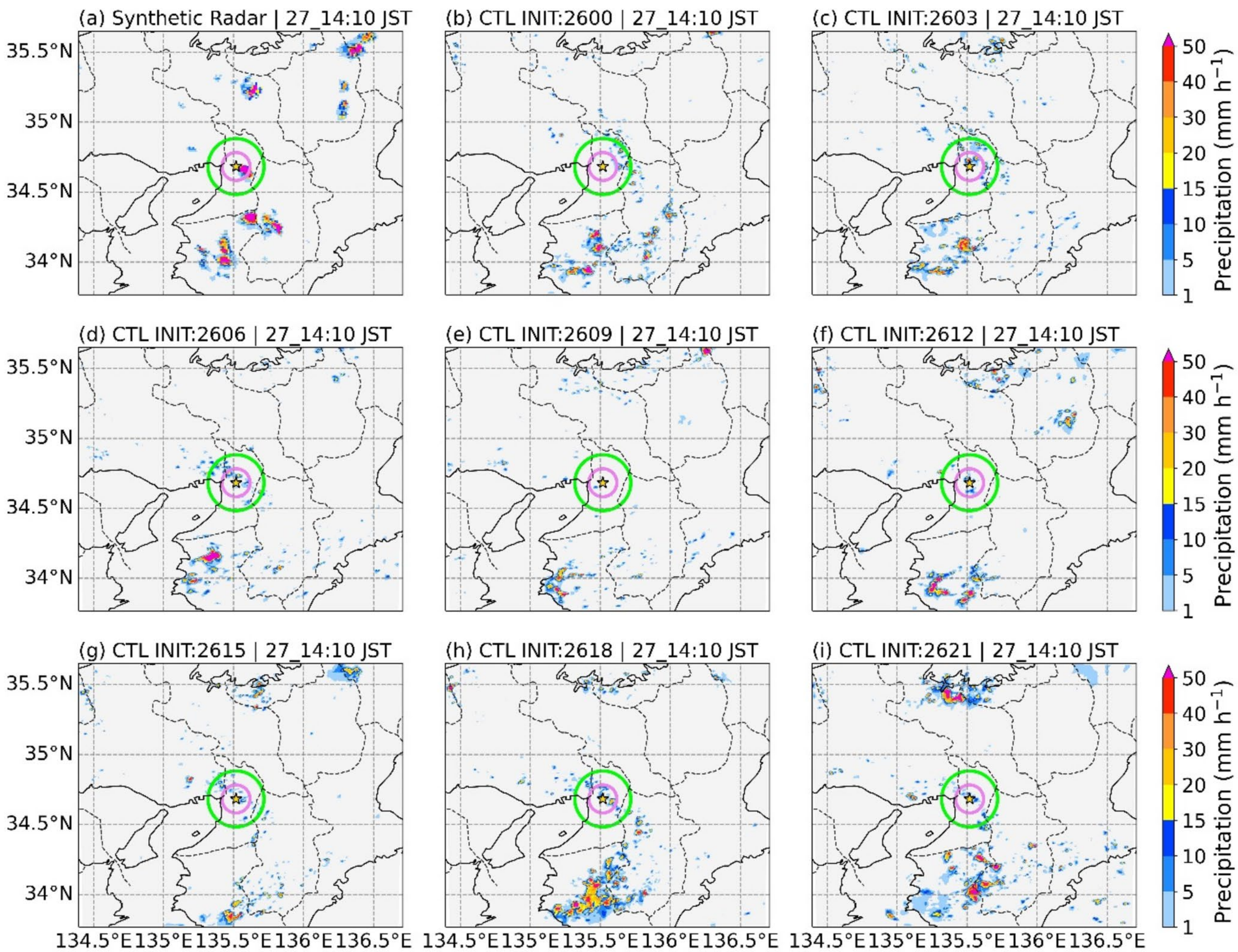

Fig. 6 The horizontal distributions of precipitation (shaded, mm h^{-1}) in (**a**) radar observation, (**b**-**i**) CTL members at 1410 JST 27 August 2023. The pink (green) circle is the R10 (R20) region and the yellow star indicates the Osaka AMeDAS point

URB-09 and URB-07 indicating the large peaks of precipitation compared to CTL, standard deviations at the time of the peaks were larger than the other experiments in URB.

We demonstrate the impacts of SHF reduction on precipitation in terms of matrices showing the ratio of accumulated and peak precipitation to CTL, calculated with ensemble mean precipitation within the R20 region, which are demonstrated in Figs. 9 and 10. The ratio is the value of the accumulated (peak) precipitation in each reduction experiment divided by that in CTL, indicating how much precipitation was reduced compared to CTL. According to the matrix of accumulated precipitation (Fig. 9), it was obvious that accumulated precipitation was more suppressed in all reduction experiments than in CTL. In all the modification regions, the ratio of accumulated precipitation showed an almost linear decreasing trend ($R^2 > 0.95$). In ALL and URB, where SHF was modified in a wide range, the decreasing trend of accumulated precipitation was greater than that in O20. O20 showed a smaller reduction trend in accumulated precipitation compared to ALL and URB. A 10% reduction in SHF in O20 showed the same degree of suppression (82%) compared to ALL and URB. In this way, the effect of modification of SHF on accumulated precipitation was clearly seen.

The matrix for peak precipitation (Fig. 10) shows that peak precipitation was reduced in almost all the reduction experiments, suggesting that modifying SHF by 50% could reduce peak precipitation to 50% or less of CTL in all modification regions. When SHF was modified from 90 to 70% of CTL, there was little difference in peak precipitation for ALL and O20, respectively. While URB-08, URB-06, and URB-05 effectively suppressed peak precipitation, URB-09 and URB-07 had greater peak precipitation than CTL. The peak precipitation did not show a discrete ratio of decrease, rather than a linear decreasing trend as was seen in the case for accumulated precipitation.

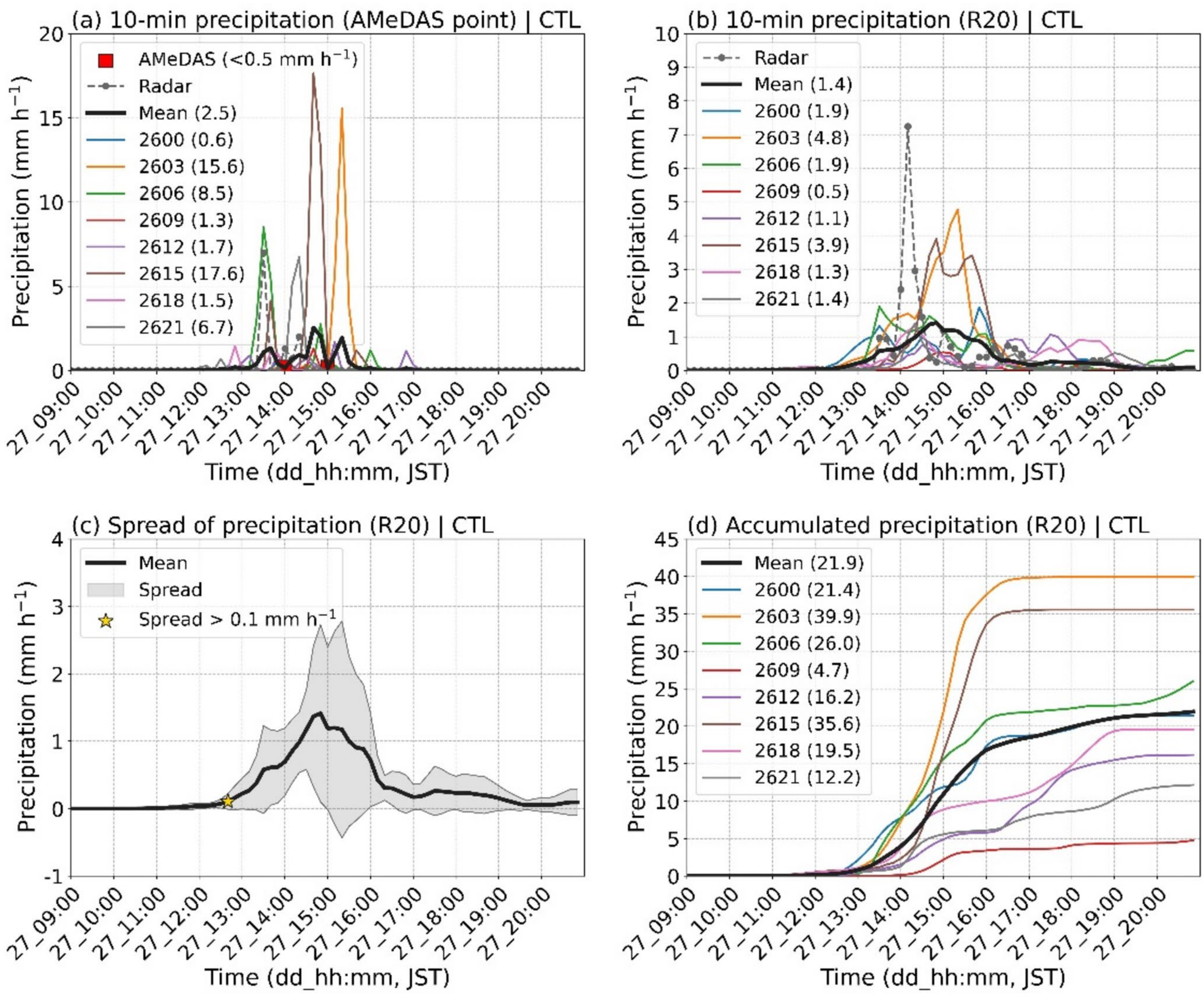

Fig. 7 The time series of precipitation in CTL (**a**) at Osaka AMeDAS point, (**b**) within the R20, (**c**) the standard deviation of the ensemble mean precipitation and (**d**) accumulated precipitation averaged over the R20. The colored lines indicate the ensemble members, the black line the ensemble mean precipitation, and the gray dotted lines indicate the radar observation. The red square marker in (**a**, **b**) indicates the time when precipitation by AMeDAS observation was over 0.5 mm h^{-1}. The yellow star in (**c**) indicates the time when the ensemble spread was over 0.1 mm h^{-1}. The values in upper left corner of each panel indicate (**a**, **b**) peak values and (**d**) accumulated amounts of precipitation

4.2 Frequency of extreme precipitation

In this subsection, the frequency distribution of precipitation for each of the 8 members consisting of each reduction experiment was further analyzed in comparison to CTL, especially focusing on extreme precipitation. The frequency distribution of precipitation was created using precipitation data within R20 from 1300 JST to 1600 JST in each reduction experiment. The spatial and temporal averaging was not applied to the results shown in this subsection. Figure 11a and c, and 11e show the frequency distribution of precipitation for ALL, URB, and O20. Precipitation greater than 99.9th percentile value of precipitation in CTL (magenta dashed line) was defined in this study as extreme precipitation. Figure 11b and d, and 11f show the sum of the frequency of the extreme precipitation.

In Figs. 11a and b, precipitation was generally reduced for all intensities in ALL compared to CTL for all the modification ratios. In URB, the frequencies around 30 mm h^{-1} in URB-09, around 50 mm h^{-1} in URB-07, and over 85 mm h^{-1} increased more than those in ALL (Fig. 11c). The frequency exceeded 100 mm h^{-1}, which rarely occurred in CTL, increased in URB-09, but the sum of the frequency of the extreme precipitation in all the modification ratios was smaller than that in CTL (Fig, 11d). In O20, unlike ALL and URB, the difference in the frequency of precipitation by modification ratios was small (Fig. 11e). The frequency of precipitation exceeded 100 mm h^{-1} was increased in

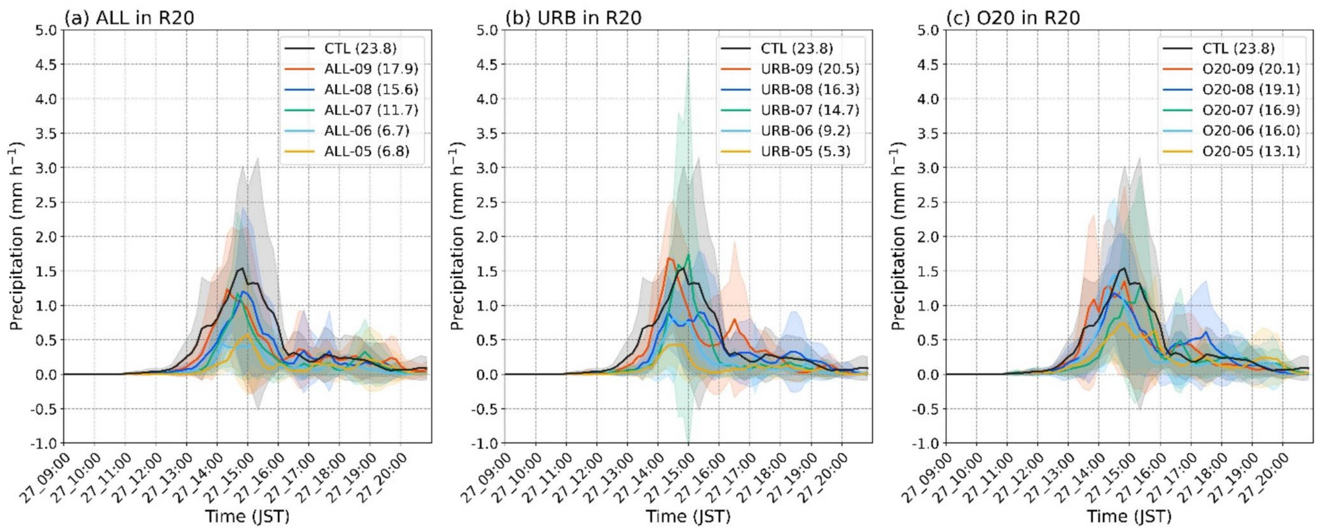

Fig. 8 Time series of precipitation averaged over urban grids in the R20 region with the ensemble mean value of (**a**) ALL, (**b**) URB, and (**c**) O20. Color shade indicates the standard deviation from ensemble mean value. The values in the upper right corner of each panel indicate the accumulated precipitation

O20-09 and O20-08 compared to CTL, while the frequency of extreme precipitation was decreased compared to CTL in all the modification ratios (Fig. 11f). The maximum values of precipitation could be suppressed in almost all the reduction experiments, although the values in ALL-08, URB-09, O20-09 and O20-08 were greater than those in CTL. As shown in Figs. 11b, d, and f, the extreme precipitation occurrences appeared differently in terms of the frequency in ALL, URB and O20 at the same modification ratios.

During the time period when the precipitation gradually increased from 1300 JST to 1600 JST (Fig. 8), the occurrence frequency of precipitation decreased in all the reduction experiments compared to CTL, indicating that the effect of SHF reduction consistently appears. It is considered that the variation in precipitation frequency among ALL, URB, and O20 (Fig. 11) would explain the non-monotonic decrease in the peak values of ensemble mean precipitation as seen in Fig. 10. Namely, changes in precipitation frequency among the ensemble members will lead to pronounced variability of the precipitation distribution among the members, resulting in large variations in the peak values of ensemble mean precipitation. In particular, an increase in moderate precipitation frequencies below the extreme threshold in URB-07 and URB-09 resulted in large peak values, even when extreme precipitation frequencies were suppressed. Thus, in order to investigate the reason for the greater peak in URB-07 and URB-09 than peak in CTL, the frequency distribution of precipitation at the peak time is shown in Fig. 12. Compared to CTL, URB-09 had a higher frequency of precipitation from 10 to 20 mm h^{-1} and a higher frequency around 30 mm h^{-1} (Fig. 12a), suggesting that ensemble mean precipitation became larger than in CTL at the time of peak precipitation. URB-07 induced a higher frequency of precipitation over 30 mm h^{-1} compared to CTL (Fig. 12a). Although the frequency of precipitation below the extreme threshold increased, the frequency of extreme precipitation decreased and the maximum value was smaller than maximum in CTL (Fig. 12b). In both cases, the precipitation was suppressed in terms of the occurrence of the extreme precipitation.

Figure 13 is a matrix showing the ratio of the 99.9th percentile value of precipitation in each reduction experiment relative to the CTL. This matrix was created using the 99.9th percentile values for each experiment, using the frequency distribution from Fig. 11. In ALL, a linear decreasing trend ($R^2 = 0.94$) was seen as the modification percentage increased, similar to the trend in accumulated precipitation. Also, URB and O20 showed a smaller decreasing trend compared to ALL ($R^2 = 0.65$ and 0.64, respectively). All types of reduction experiments exhibited smaller extreme precipitation than that in CTL, suggesting a suppressive effect of reducing SHF on extreme and 99.9th percentile precipitation.

5 Discussion

Steadily reducing SHF relative to the CTL case reduced the intensity and frequency of precipitation. In this section, additional analyses are performed to understand the mechanism behind this reduction of precipitation.

First, the impact of SHF reduction on the atmosphere was examined. Since less SHF reduced the energy received at the height of the lowest level of the model (Z_0, approximately

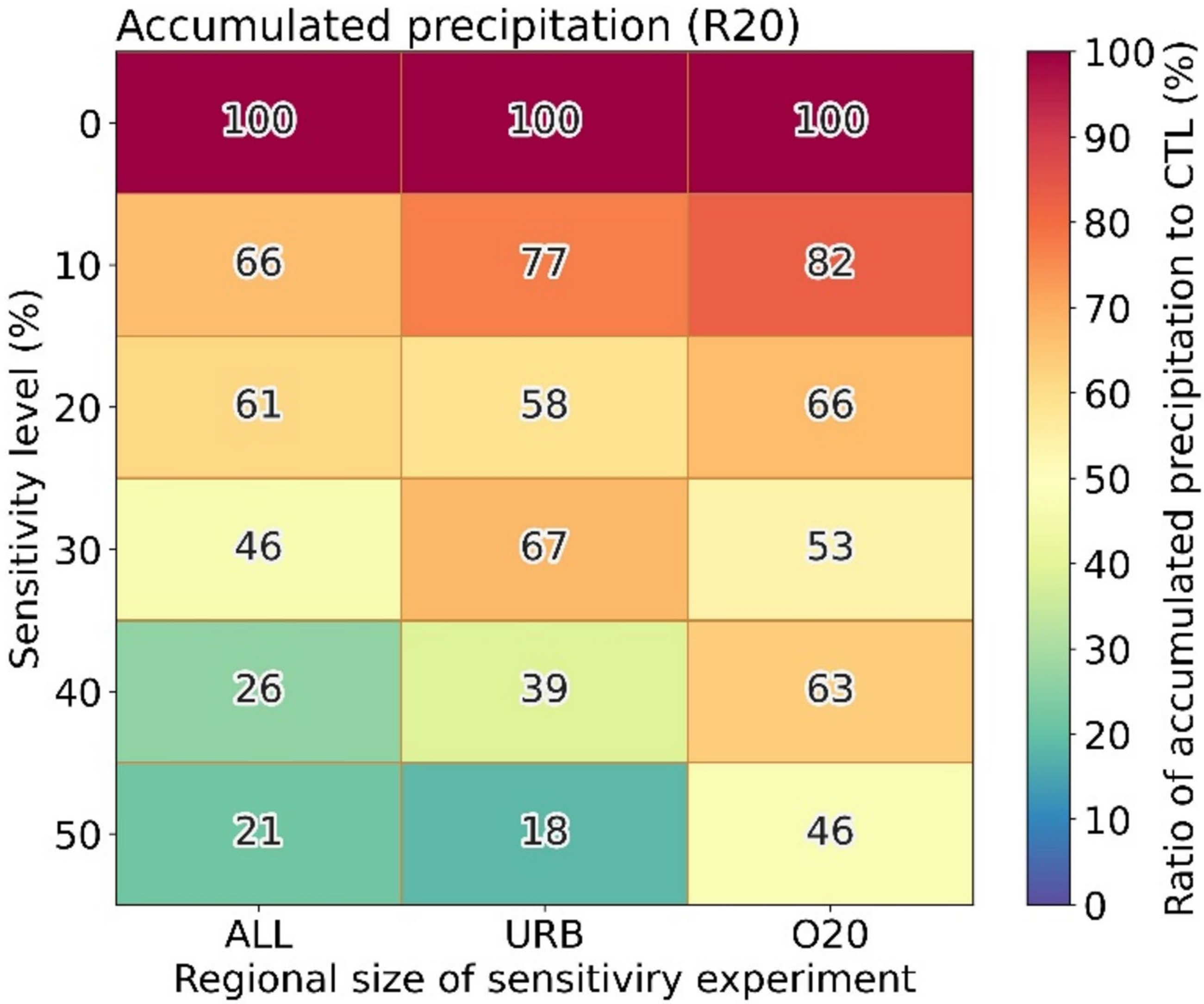

Fig. 9 Matrix of the ratio of the accumulated precipitation between CTL and reduction experiments (colored). The vertical axis is the reduction level of SHF and horizontal axis is the modification region

55 m), the temperature at Z_0 was expected to decrease in response to the magnitude of SHF. Figures 14a-c show the time series of ensemble mean temperature at Z_0 averaged over R20. Ensemble mean temperature at Z_0 peaked in the afternoon and began to decrease when ensemble mean precipitation peaked (Fig. 8). It is seen in Fig. 14 that the temperature at Z_0 in the morning hours was largely lowered with the SHF modifications in ALL and URB but it was not so much reduced in O20. This difference between ALL/URB and O20 experiments was considered to be related to the area size of the reduction region and the degree of reduction level. A wider modification region reduced the energy transfer to the atmosphere over a wider area. In addition, there was no difference in temperature at the upper levels (e.g., height of 3000 m and 5000 m) in all the reduction experiments (not shown), suggesting that the troposphere became more stabilized with the modification region and ratio.

Figures 14d-f show the time series of vertically accumulated cloud water mixing ratio (Q_c) averaged over R20. The temporal variation of Q_c changed almost in phase with ensemble mean precipitation (Fig. 8), indicating that the stabilized atmosphere efficiently suppressed the development and formation of clouds. These results suggested that SHF modification stabilized the atmosphere by decreasing the energy transfer from the ground to the atmosphere, resulting in a reduction of precipitation by suppressing the development of clouds. However, standard deviations of Q_c were large in URB and O20, suggesting that among the ensemble there were some members that promoted or inhibited cloud development.

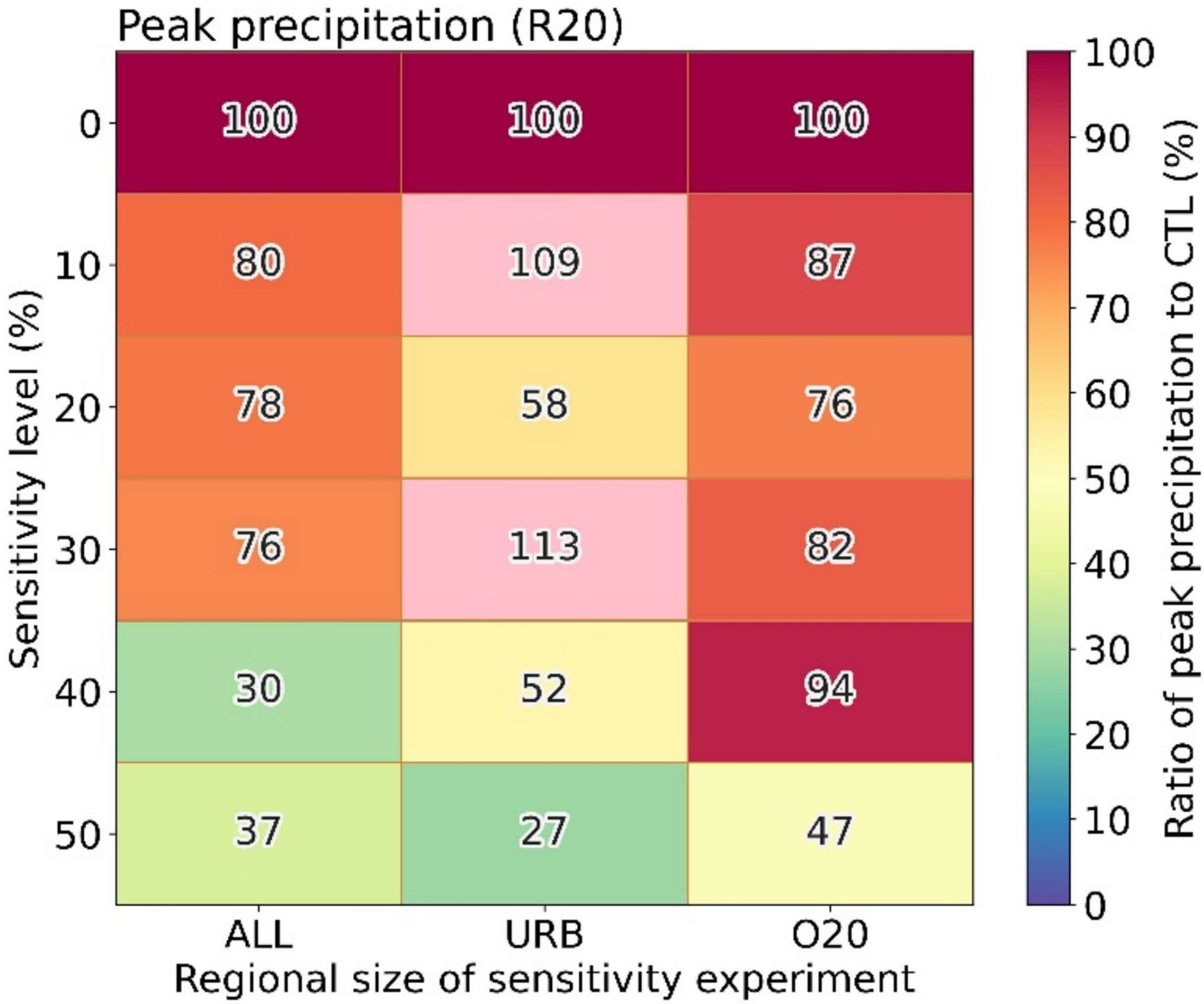

Fig. 10 As in Fig. 9 except for the peak of precipitation. The pink panels indicate the ratio of peak precipitation in reduction experiment against that in CTL is over 100%

Second, the atmospheric stability that changed owing to the decrease in temperature at Z_0 will be examined. Figure 15 indicates the temporal variations of the static stability in the lower troposphere. Here we examine the difference in temperature between Z_{14} (the 14th layer of the model, approximately 1500 m) and Z_0, i.e., the lower tropospheric static stability, which will be referred to as LOWSTB hereafter. LOWSTB is represented as following equation:

$$LOWSTB = T_{14} - T_0 \tag{1}$$

where T_{14} is the temperature at Z_{14} and T_0 is the temperature at Z_0. Note that a larger absolute number of LOWSTB means a decreased stability, or the increased instability. The reference time for the beginning of precipitation is 1300 JST, when the spread of precipitation begins to expand (Fig. 7c). The value of LOWSTB gradually decreased until 1300 JST, when the amount of precipitation began to increase in the CTL (Fig. 15a). This indicates that LOWSTB decreased before the beginning of precipitation. After 1300 JST, the amount of precipitation increased and LOWSTB gradually increased. In order to investigate the decrease in precipitation and the atmospheric stability, the differences of LOWSTB and precipitation between CTL and each reduction experiments were computed. In ALL, difference of LOWSTB decreased as the reduction level increased before the beginning of precipitation in the CTL (i.e., the atmosphere stabilized). Thus, the difference in precipitation increased (i.e. precipitation decreased), and precipitation decreased when the reduction level was large. The similar characteristics were also found in URB. Namely, LOWSTB decreased and the difference in precipitation increased

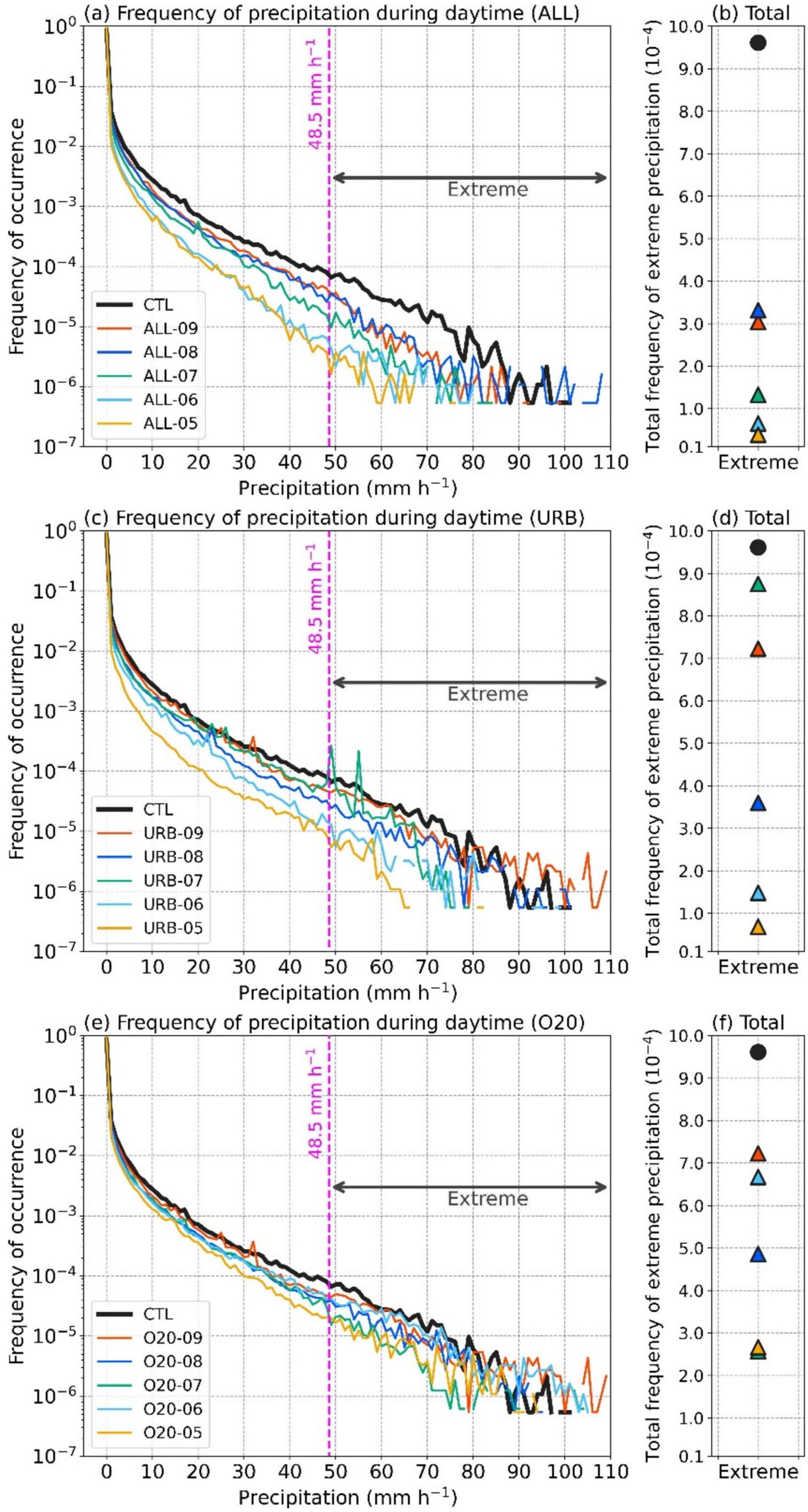

Fig. 11 The frequency of occurrence for precipitation over urban grids within R20 during daytime in (**a**) ALL, (**b**) URB, and (**c**) O20. The black solid line shows CTL and colored lines the reduction experiments. The dashed magenta line indicates the 99.9th percentile value of precipitation in CTL. The black dots and colored triangles indicate the sum of the frequency for the extreme precipitation in CTL, (**b**) ALL, (**d**) URB, and (**f**) O20, respectively

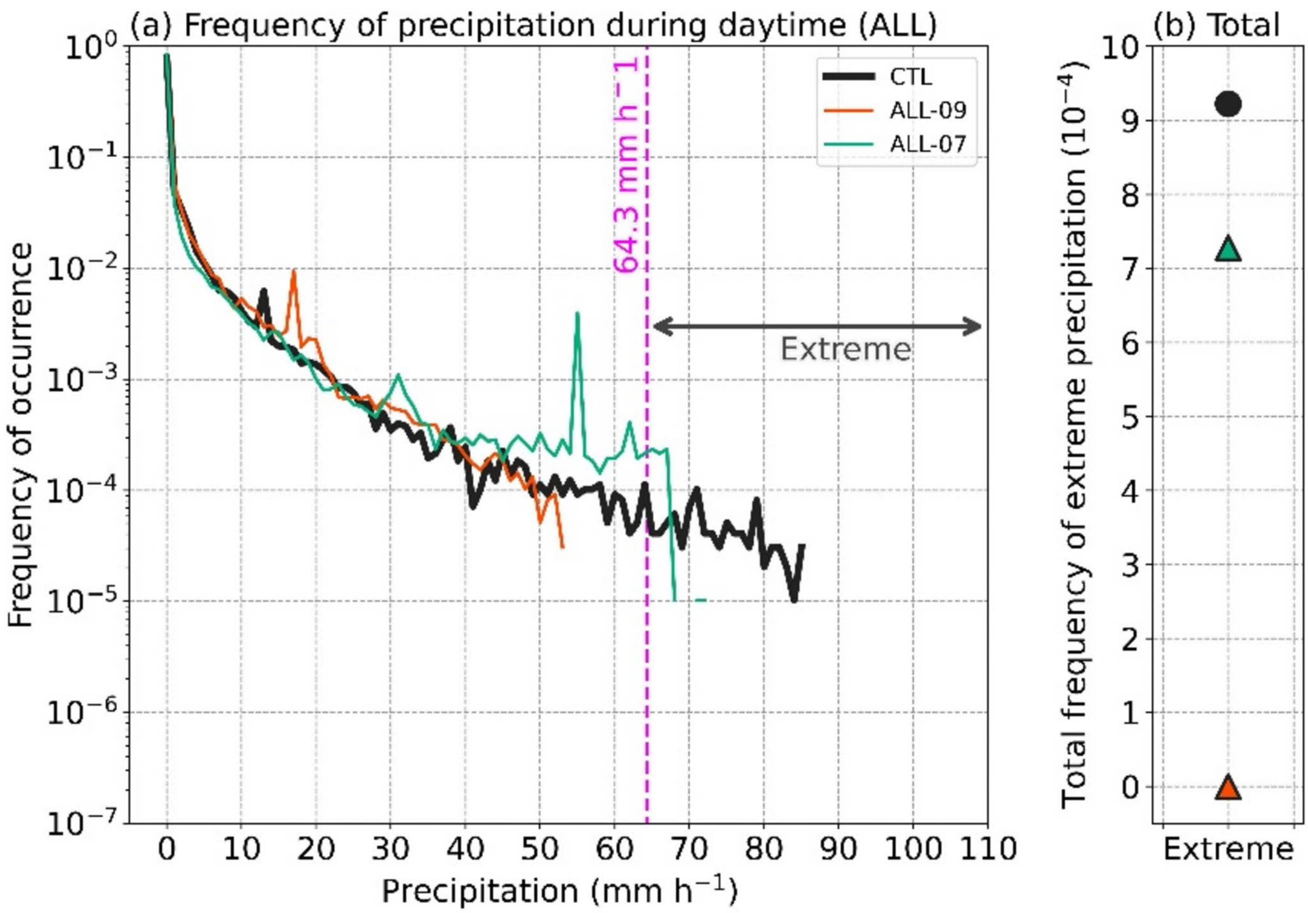

Fig. 12 As in Fig. 11 except for the frequency against the precipitation intensity at the time of peak precipitation in CTL, URB-09, and URB-07

when the reduction level was large. In O20, the difference in LOWSTB was smaller than that in ALL and URB, while the pattern of a decrease in LOWSTB was similar to that in ALL and URB. Therefore, it was suggested that a decrease in precipitation was caused by an increase in atmospheric stability due to the decrease in SHF.

Considering that the moist convection could be enhanced by heat transfer from urban areas (which would strengthen the upward motion) (Han and Baik 2008), the reduction of precipitation in the modified experiments can be explained by the suppression of vertical motions. Figure 16 shows the 99th percentile and mean values of vertical winds between Z_0 and the height of Z_{14}. The former was computed from the values of vertical wind in all grids in R20 from Z_0 to Z_{14} between 1300 JST and 1600 JST, and the latter was their average. The absolute values of the vertical winds below Z_{14} were smaller in both the 99th percentile value and the average value, depending on the reduction level, because convection was suppressed by the reduction in atmospheric stability. Therefore, the results of this study suggest that an increase in atmospheric stability due to less SHF inhibits convective development and consequently reduces precipitation.

This study suggested that a steady decrease in SHF may contribute to reducing accumulated and peak precipitation and also reducing the occurrence frequency of extreme precipitation. However, SHF modifications might not be effective at predicting instantaneous precipitation rates, such as a maximum value of precipitation. In some cases, a reduction in SHF did not necessarily lead to a decrease in the frequency or intensity of extreme precipitation. Although precipitation was difficult to control in certain scenarios, the results indicate the possibility that steady SHF reduction can reduce precipitation under specific conditions. Nevertheless, in the case examined in this study—an isolated and scattered precipitation event—the model also exhibited limited skill in reproducing the observed precipitation distribution. This suggests that other sources of error, such as model deficiencies or uncertainties in the initial conditions, may overshadow the impact of the SHF reduction. Data assimilation may be necessary to accurately reproduce the precipitation distribution shown in Fig. 1. Further efforts are required

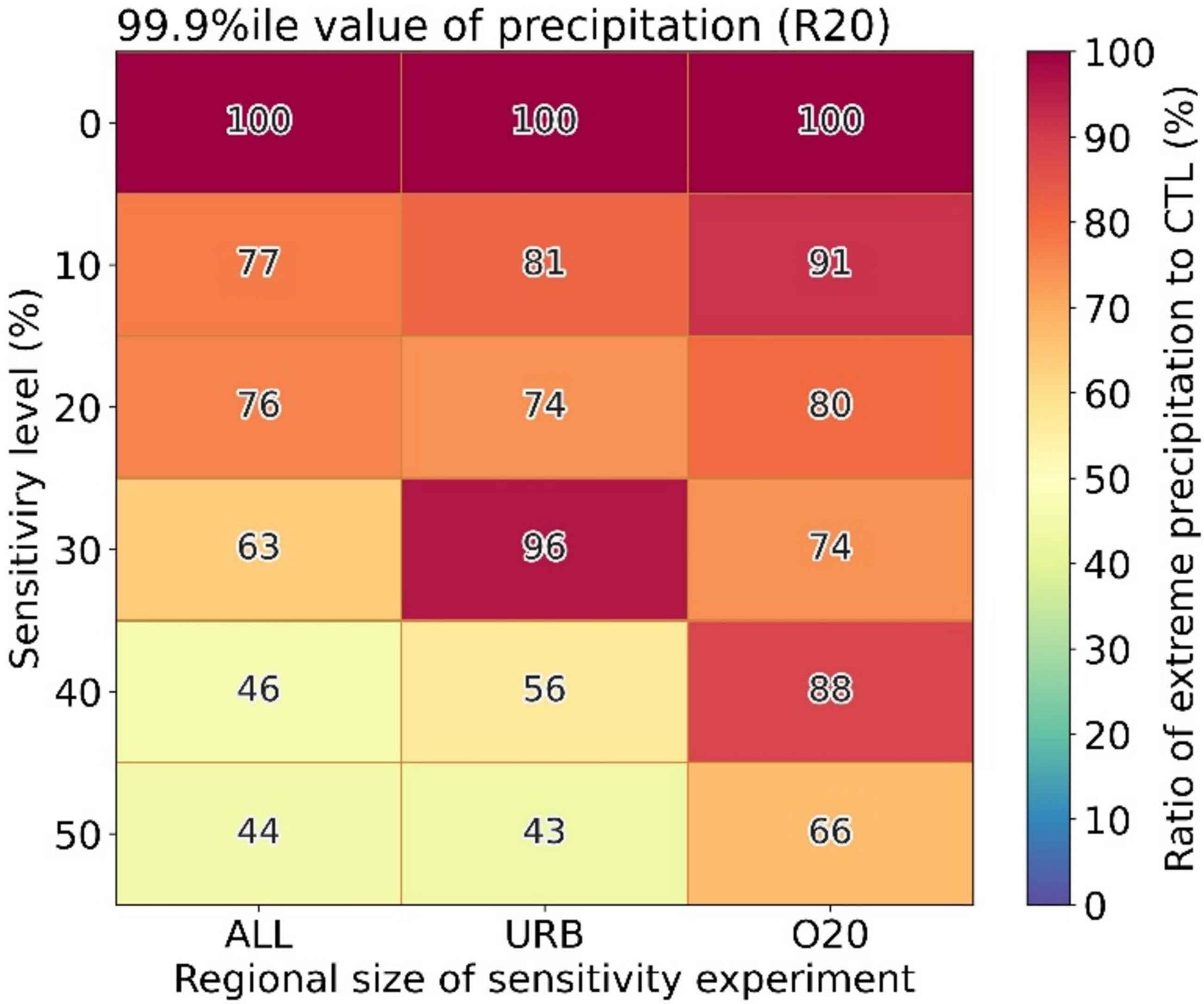

Fig. 13 As in Fig. 9 except for the extreme precipitation

to improve the control simulation before drawing definitive conclusions about the effects of the SHF reduction.

Although steady reduction of SHF was examined in this study, it is essential to identify an appropriate time and place to modify SHF for effectively reducing precipitation with a more realistic artificial intervention. In addition, a more accurate examination of urban precipitation will require an assessment of precipitation modifications through simulations that reflect the detailed characteristics of each urban area (e.g., building height, and building density), such as the Local Climate Zone (Stewart and Oke 2012). In this study, the urban surface conditions were reproduced without using the Urban Canopy Model (e.g., Kusaka et al. 2001; Martilli et al. 2002), but using the Urban Canopy Model would easily reduce the sensible heat flux from the urban surface. We consider that combining it with the LCZ would provide an even more realistic experimental setting. Furthermore, the required number of ensemble members, which is a potential issue of the experiment, should be explored in the future with large ensemble members to quantify the uncertainty of precipitation simulations, like an approach employed by Kusaka et al. (2014). Finally, as a problem arising from weather modification, a crucial question of whether society will tolerate the possibility of unexpected extreme precipitation shown by the results of this study is also an important factor to consider in the future.

6 Summary

We investigated the effect of sensible heat flux (SHF) modification on precipitation in cumulonimbus clouds that developed on a specific summertime afternoon. Due to the random and chaotic nature of these phenomena, the

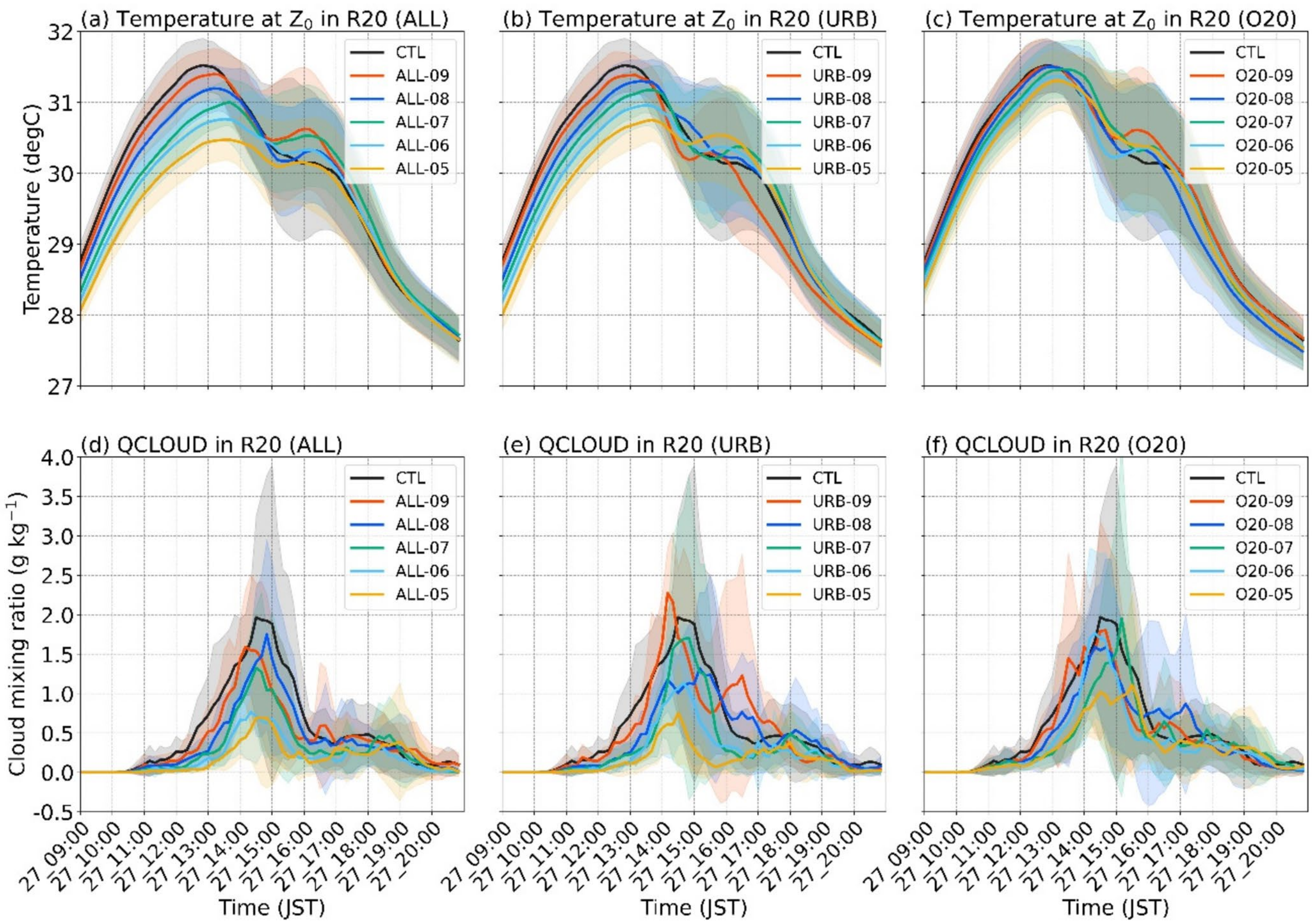

Fig. 14 (**a-c**) Time series of temperature (°C) at the Z_0, and (**d-f**) vertically accumulated cloud water mixing ratio (g kg^{-1}) averaged over R20 with only urban grids. The black line indicates the ensemble mean of CTL and the colored lines indicate the ensemble mean of reduction experiments. Color shade indicates the standard deviation from ensemble mean value

location and time of precipitation occurrence significantly vary among ensemble members. To account for this variability, we conducted ensemble simulations with different initial times and created 8 ensemble members. This study examined a local-scale afternoon precipitation event that occurred in Osaka, Japan. The control experiments (CTL) successfully reproduced precipitation with a peak in the afternoon over the urban area of Osaka.

In order to investigate the effect of reducing SHF on precipitation, the reduction experiment was performed by changing the reduction level and region. The reduction level was varied from 10 to 50% in 10% increments, and the reduction region was set as follows: the entire D03 (ALL), only the urban grid of the entire D03 (URB), and only the urban grid within a 20 km box centered the Automated Meteorological Data Acquisition System (AMeDAS) point in Osaka (O20). For example, ALL-05 represents the experiment of ALL area with a 50% reduction level. These settings assumed that the urban area remained unchanged from the land use category and that artificial intervention mitigate the urban effect.

Each reduction experiment reproduced precipitation with a peak in the afternoon similar to CTL. The potential for modifying peak and accumulated precipitation was evaluated by comparing ensemble mean precipitation between reduction experiments and CTL. Accumulated precipitation decreased in all the reduction experiments compared to CTL. The peak precipitation also decreased in almost all the

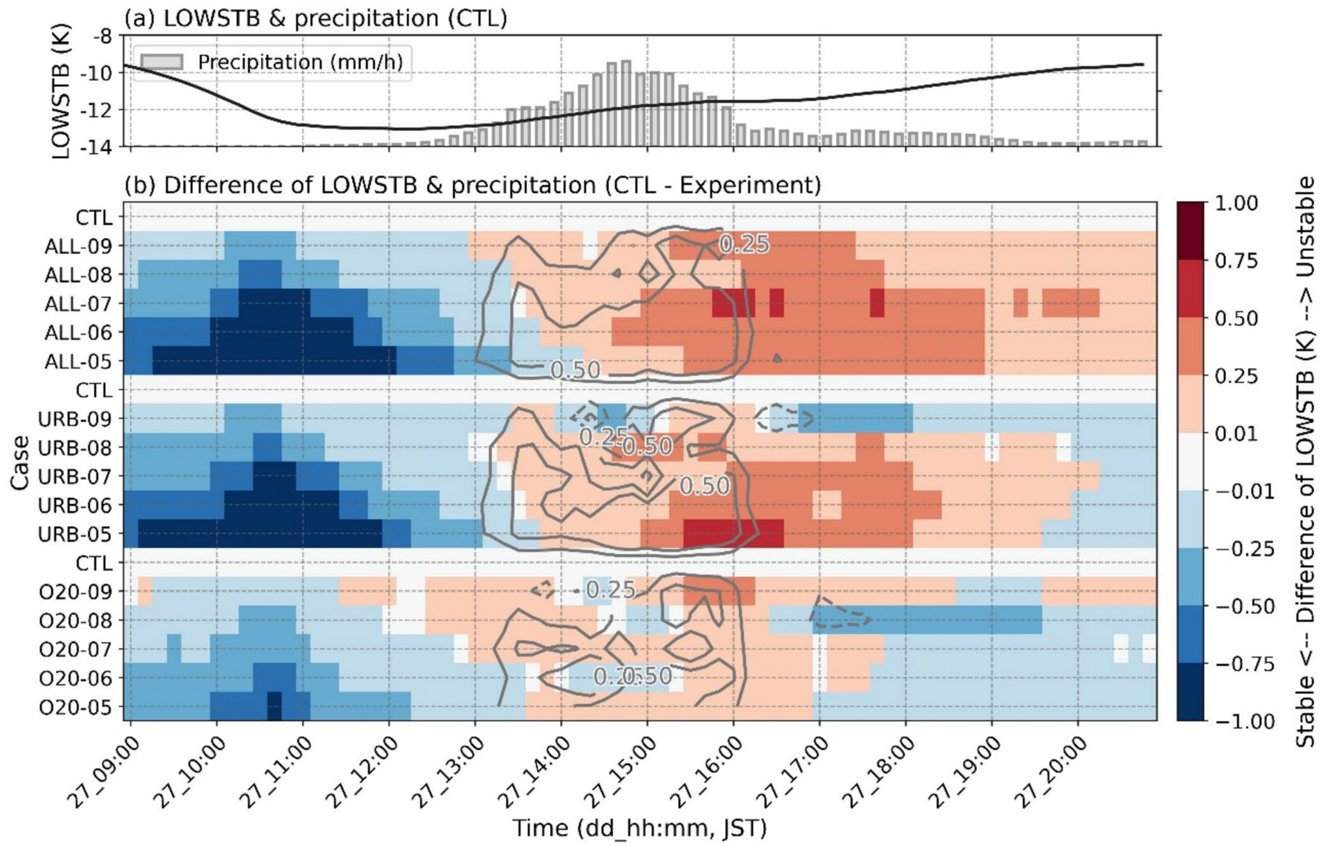

Fig. 15 Time series of (**a**) LOWSTB (solid line, K) and precipitation averaged over the R20 region (bar, mm h^{-1}) in the CTL, and (**b**) the difference of LOWSTB (colored, K) and precipitation (contour, mm h^{-1}) between CTL and reduction experiments

experiments, although it increased in URB-09 and URB-07. The frequency of occurrence of extreme precipitation which was defined as the 99.9th percentile value of precipitation in CTL, also decreased in most experiments, although the maximum precipitation value was larger than that of CTL in some experiments. This research is valuable because we provided a new perspective that has not been explored in previous studies: directly reducing the sensible heat flux from the surface in existing urban areas leads to a decrease in precipitation.

These results suggest that steady decrease in SHF can effectively suppress precipitation. The reduction in precipitation may result from a series of processes: the SHF reduction decreased the energy received by the lowest atmospheric layers, resulting in a stabilization of the atmosphere due to lower temperatures, and thus the suppression of cloud development. The stabilization of the atmosphere weakened vertical winds, and the cloud formation was suppressed as indicated by the reduced cloud water mixing ratio.

This study is meaningful regarding future artificial heat intervention operations because of quantitatively evaluates the decrease in precipitation. In the most practical intervention scenario within the current experimental setup, O20-09, the ensemble mean accumulated precipitation decreased by 18%, the ensemble mean peak precipitation decreased by 13%, and the value of the 99.9th percentile precipitation decreased by 9%. Therefore, this study quantitatively demonstrates the potential for precipitation suppression through SHF reduction.

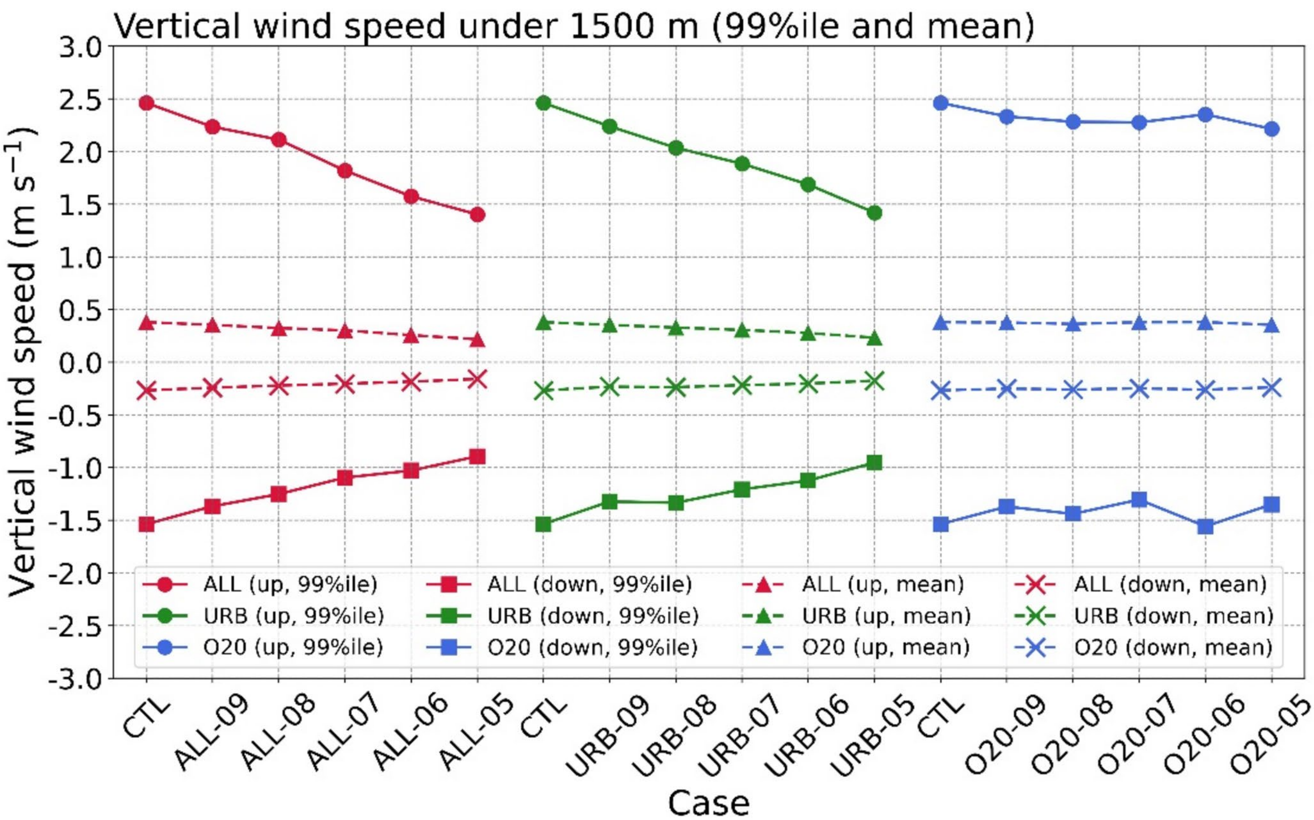

Fig. 16 The 99th percentile (solid line) and mean (broken line) values of vertical wind speeds between Z_0 and the height of 1500 m during daytime in R20 with urban grids. Colors show the reduction experiments. Circle (square) markers indicate the 99.9th percentile value of upward (downward) winds and triangle (cross) markers indicate the mean value of upward (downward) winds

Acknowledgements We are grateful to Dr. Takuya Kawabata and Dr. Pin-Ying Wu of the Meteorological Research Institute for discussions to advance this research. This research was supported by JST for Moonshot R&D Program Grant Number JPMJMS2283. The Digital Map 50 m Grid (Elevation) data was obtained from the Geospatial Information Authority of Japan. The 10-km mesh synthetic radar grid point value data were provided by the database of the Research Institute for Sustainable Humanosphere, Kyoto University. The ERA5 were obtained from ECMWF.

Author contributions All authors contributed to the conception and design of the study. K. Irie and T. Takemi performed material preparation, data collection, and analysis. K. Irie, wrote the first draft of the manuscript and T. Takemi commented on previous versions of the manuscript. All authors read and approved the final manuscript.

Funding This research was supported by JST for Moonshot R&D Program Grant Number JPMJMS2283.

Data availability All data of the ensemble experiments by the WRF model and the modified module_sf_noahlsm.F code used for the SHF modification experiments are available upon request. The GIA50 data were obtained from the Geospatial Information Authority of Japan: https://fgd.gsi.go.jp/download/mapGis.php. The ERA5 data were obtained from the Copernicus Climate Change Service: Pressure levels: https://cds.climate.copernicus.eu/cdsapp#!/dataset/reanalysis-era5-pressure-levels? tab=overview, Single levels: https://cds.climate.copernicus.eu/cdsapp#!/dataset/reanalysis-era5-single-levels? tab=overview. The synthetic radar data were obtained from the database of the Research Institute for Sustainable Humanosphere, Kyoto University: http://database.rish.kyoto-u.ac.jp/arch/jmadata/data/jma-radar/synthetic/original/.

Code availability The modified module_sf_noahlsm.F code is available upon request.

Declarations

Ethical approval Not applicable.

Consent to participate Not applicable.

Consent for publication Not applicable.

Competing interests The authors declare no competing interests.

References

Aligo EA, Gallus WA Jr, Segal M (2009) On the impact of WRF model vertical grid resolution on Midwest summer rainfall forecasts. Wea Forecast 24:575–594. https://doi.org/10.1175/2008WAF2007101.1

Bornstein R, Lin Q (2000) Urban heat Islands and summertime convective thunderstorms in Atlanta: three case studies. Atmos Env 34:507–516. https://doi.org/10.1016/S1352-2310(99)00374-X

Changon SA Jr, Huff FA, Semonin RG (1971) METROMEX: an investigation of inadvertent weather modification. Bull Amer Meteor Soc 52:958–968. https://doi.org/10.1175/1520-0477(1971)052%3C0958:MAIOIW%3E2.0.CO;2

Doan Q-V, Chen F, Kusaka H, Wang J, Kajino M, Takemi T (2022) Identifying a new normal in extreme precipitation at a City scale under warmer climate regimes: A case study of the Tokyo metropolitan area, Japan. J Geophys Res Atmos 127 e2022JD036810. https://doi.org/10.1029/2022JD036810

Fujibe F (1998) An increasing trend of extremely hot days in the inland of the Kanto plain and its relation to urban effects. Tenki 45:643–653 (in Japanese with English abstract)

Fujibe F, Togawa H, Sakata M (2009) Long-term change and Spatial anomaly of warm season afternoon precipitation in Tokyo. SOLA 5:17–20. https://doi.org/10.2151/sola.2009-005

Han J-Y, Baik J-J (2008) A theoretical and numerical study of urban heat Island–induced circulation and convection. J Atmos Sci 65:1859–1877. https://doi.org/10.1175/2007JAS2326.1

Hersbach H, Bell B, Berrisford P, Hirahara S, Horányi A, Muñoz-Sabater J et al (2020) The ERA5 global reanalysis. Quart J Roy Meteor Soc 146:1999–2049. https://doi.org/10.1002/qj.3803

Kanda M (2007) Progress in urban meteorology: A review. J Meteor Soc Japan 85B:363–383. https://doi.org/10.2151/jmsj.85B.363

Kusaka H, Kimura F, Hirakuchi H, Mizutori M (2000) The effects of land-use alteration on the sea breeze and daytime heat Island in the Tokyo metropolitan area. J Meteor Soc Japan 78:405–420. https://doi.org/10.2151/jmsj1965.78.4_405

Kusaka H, Kondo H, Kikegawa Y, Kimura F (2001) A simple single-layer urban canopy model for atmospheric models: comparison with multi-layer and slab models. Bound -Layer Meteor 101:329–358. https://doi.org/10.1023/A:1019207923078

Kusaka H, Nawata K, Suzuki-Parker A, Takane Y, Furuhashi N (2014) Mechanism of precipitation increase with urbanization in Tokyo as revealed by ensemble climate simulations. J Appl Meteor Climatol 53:824–837. https://doi.org/10.1175/JAMC-D-13-065.1

Martilli A, Clappier A, Rotach M (2002) An urban surface exchange parameterization for mesoscale models. Bound -Layer Meteor 104:261–304. https://doi.org/10.1023/A:1016099921195

Matheson AM, Ashie Y (2008) The effect of changes of urban surfaces on rainfall phenomenon as determined by non-hydrostatic mesoscale model. J Meteor Soc Japan 86:733–751. https://doi.org/10.2151/jmsj.86.733

Nomura S, Takemi T (2011) Environmental stability for afternoon rain events in the Kanto plain in summer. SOLA 7:9–12. https://doi.org/10.2151/sola.2011-003

Oke TR, Mills G, Christen A, Voogt JA (2017) Urban climates, 546pp. edn. Cambridge University Press. https://doi.org/10.1017/9781139016476

Quattrochi DA, Luvall jC, Estes MG, lo CP, Kidder SQ, Hafner J, Taha H, Bornstein RD, Gillies RR, Gallo KP (1998): Project ATLANTA (Atlanta Land Use Analysis: Temperature and Air Quality) – A study of how the urban landscape affects meteorology and air quality through time. Preprints, *Second Urban Environment Conf.*, Albuquerque, NM, Amer. Meteor. Soc., 104–107

Seino N, Aoyagi T, Tsuguti H (2018) Numerical simulation of urban impact on precipitation in Tokyo: how does urban temperature rise affect precipitation? Urban Clim 23:8–35. https://doi.org/10.1016/j.uclim.2016.11.007

Shem W, Shepherd M (2009) On the impact of urbanization on summertime thunderstorms in Atlanta: two numerical model case studies. Atmos Res 92:172–189. https://doi.org/10.1016/j.atmosres.2008.09.013

Shimadera H, Kondo A, Shretha KL, Kitaoka K, Inoue Y (2015) Numerical evaluation of the impact of urbanization on summertime precipitation in Osaka, Japan. Adv Meteor. 10 pp.https://doi.org/10.1155/2015/379361

Skamarock WC, Coauthors (2019): A description of the Advanced Research WRF Model version 4. NCAR Tech. Note NCAR/TN–556+STR, 145 pp., https://figshare.com/articles/journal_contribution/A_Description_of_the_Advanced_Research_WRF_Version_4/7369994?file=14057147

Statistics Bureau of Japan (2025): *Japan statistical yearbook*, Ministry of Internal Affairs and Communications. https://www.stat.go.jp/english/data/nenkan/index.html

Steensen BM, Marelle L, Hodnebrog Ø, Myhre G (2022) Future urban heat Island influence on precipitation. Clim Dyn 58:3393–3403. https://doi.org/10.1007/s00382-021-06105-z

Stewart ID, Oke TR (2012) Local climate zones for urban temperature studies. Bull Am Meteor Soc 93:1879–1900. https://doi.org/10.1175/BAMS-D-11-00019.1

Takemi T (2009a) High-resolution numerical simulations of surface wind variability by resolving small-scale terrain features. Theor Appl Mech Japan 57:421–428. https://doi.org/10.11345/nctam.57.421

Takemi T (2009b) High-resolution simulation of the 28 July 2008 heavy rain events over the Kinki and Hokuriku area. Annuals of Disas. Prev. Res. Inst, Kyoto Univ., No. 52 B, pp. 421–429, (in Japanese with English abstract). http://hdl.handle.net/2433/129304

Takemi T (2014) Characteristics of summertime afternoon rainfall and its environmental conditions in and around the Nobi plain. SOLA 10:158–162. https://doi.org/10.2151/sola.2014-033

Takemi T (2018) Importance of terrain representation in simulating a stationary convective system for the July 2017 Northern Kyushu heavy rainfall case. SOLA 14:153–158. https://doi.org/10.2151/sola.2018-027

Takemi T, Ito R (2020) Benefits of high-resolution downscaling experiments for assessing strong wind hazard at local scales in complex terrain: a case study of typhoon Songda (2014). Prog Earth Planet Sci 7(4):1–16. https://doi.org/10.1186/s40645-019-0317-7

Takemi T, Yoshida T, Horiguchi M, Vanderbauwhede W (2020) Large-Eddy-simulation analysis of airflows and strong wind hazards in urban areas. Urban Clim 32:100625. https://doi.org/10.1016/j.uclim.2020.100625

Yamamoto Y, Ishikawa H (2020) Influence of urban spatial configuration and sea breeze on land surface temperature on summer clear-sky days. Urban Clim 31:100578. https://doi.org/10.1016/j.uclim.2019.100578